Final technical report

Grant name: Temple University of the Commonwealth System
Grant Number: DE-SC0004764
Title of the Grant: Enhancement of spin-lattice coupling in nanoengineered oxide films and heterostructures by laser MBE
Period of Performance: 7/1/2010 to 1/31//2017
PI's Name: Xiaoxing Xi

Program Scope

The objective of the proposed research is to investigate nanoengineered oxide films and heterostructures that are predicted to show desirable physical properties. The main focus of the project is short-period superlattices grown by atomic layer-by-layer laser MBE from separate oxide targets (for example, growing $SrTiO_3$ from SrO and TiO_2 targets). The atomic layer-by-layer mode of the laser MBE growth is superior to the conventional laser MBE in broadening the thermodynamic space for the synthesis of short-period superlattices and new designer materials.

Recent Progress

1. Atomic Layer-by-Layer Laser MBE

The principle of ALL-Laser MBE is schematically illustrated in Fig. 1A. Separate oxide targets are used – instead of using a compound target of $SrTiO_3$, targets of SrO and TiO_2 are switched back and forth as they are alternately ablated by a UV laser beam. In conventional PLD or laser MBE using a compound target, all elements are ablated at once and the film grows unit cell by unit cell. In ALL-Laser MBE using separate targets, on the other hand, the film is constructed one atomic layer at a time.

Figure 1B shows the RHEED intensity oscillations as the targets of SrO and TiO_2 are alternately ablated. When Sr/Ti > 1 the peak intensity increases and a "double" peak appears. When Sr/Ti < 1 the peak intensity decreases. When Sr/Ti = 1 the intensity and shape of the oscillation peaks are constant. Furthermore, insufficient or excess pulses in each cycle cause RHEED intensity beating (Fig. 1C) while it remains constant for 100% layer coverage (Fig. 1D).

ALL-Laser MBE is versatile: it works for non-polar film on non-polar substrate (homoepitaxy of $SrTiO_3$), polar film on polar substrate ($La_5Ni_4O_{13}$ on $LaAlO_3$), and polar film on non-polar substrate ($LaAlO_3$ on $SrTiO_3$). It allows one to push the

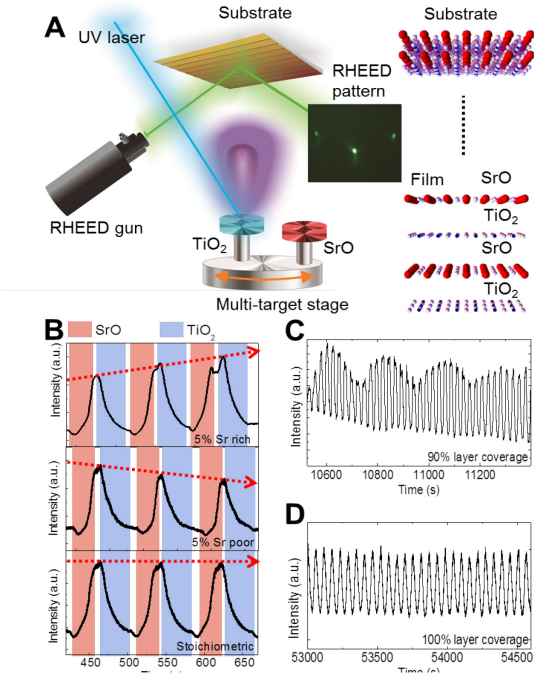

Figure 1 (**A**) Schematic of ALL-Laser MBE. (**B**) RHEED diffracted spot intensity during the atomic layer-by-layer growth of $SrTiO_3$ films for the cases of Sr-rich, Sr-poor, and stoichiometric deposition, respectively. (**C**) RHEED intensity beating when 0.9 monolayers of SrO and TiO_2 are deposited during each target switching cycle. (**D**) RHEED intensity oscillations for a stoichiometric sample with full layer coverage.

thermodynamic boundary further in stabilizing new phases than reactive MBE and PLD. For example, $La_5Ni_4O_{13}$, the Ruddlesden-Popper phase with $n = 4$, has never been reported in the literature because it needs atomic layer-by-layer growth at high oxygen pressures, not possible with other growth techniques. ALL-Laser MBE makes it possible.

2. Mechanism of the 2D Electron Gas at $LaAlO_3/SrTiO_3$ Interface

Since the discovery of the interfacial 2D electron gas in the $LaAlO_3/SrTiO_3$ system,[1] its mechanism has been a subject of controversy. According to the electronic reconstruction mechanism, because the atomic layers are charge neutral in $SrTiO_3$ but charged in $LaAlO_3$, a positive diverging electric potential is built up in a $LaAlO_3$ film grown on a TiO_2-terminated $SrTiO_3$ substrate. This leads to the transfer of half of an electron from the $LaAlO_3$ film surface to $SrTiO_3$ when the $LaAlO_3$ layer is thicker than 4 unit cells, creating a 2D electron gas at the interface with a sheet carrier density of $3.3\times10^{14}/cm^2$ for sufficiently thick $LaAlO_3$.[2] A serious inconsistency with this mechanism is that the carrier densities reported experimentally are invariably lower than the expected value[2] except under conditions where reduction of $SrTiO_3$ substrate is suspected.[3] Oxygen vacancies in $SrTiO_3$ are known to contribute to conductivity, but all reported conducting $LaAlO_3/SrTiO_3$ interfaces have been grown at low oxygen pressures (< 10 mTorr), and annealing in oxygen is often required; higher oxygen pressures during the PLD growth result in insulating samples or 3D island growth.[4]

Because we grow the $LaAlO_3$ film one atomic layer at a time, we were able to grow conducting $LaAlO_3/SrTiO_3$ interfaces at a high oxygen pressure with ALL-Laser MBE. Starting from a TiO_2-terminated $SrTiO_3$ substrate, we grew 10 unit-cell-thick $LaAlO_3$ films by alternately ablating La_2O_3 and Al_2O_3 targets under an oxygen pressure of 37 mTorr. Furthermore, we grew $LaAlO_3$ films of different cation stoichiometry, $LaAl_{1+y}O_{3(1+0.5y)}$, by varying the number of laser pulses on the Al_2O_3 target. The RHEED intensity oscillations during the growth of a stoichiometric film are shown in Fig. 2A. The RHEED intensity remain close to the substrate level throughout the growth. The 2D growth was also confirmed by the sharp RHEED spots in Fig. 2B for the 10 unit-cell film. The AFM image for the film in Fig. 2C shows an atomically flat surface.

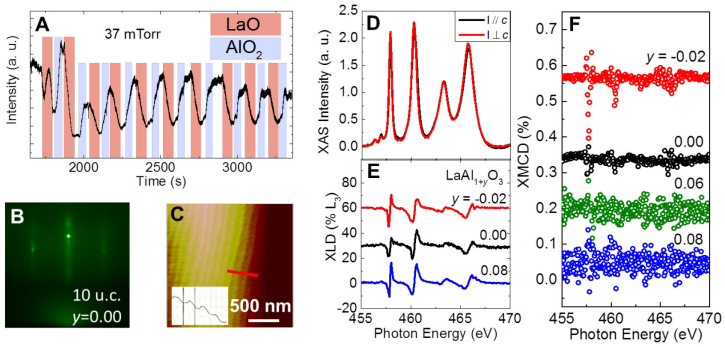

Figure 2 (**A**) RHEED intensity oscillation during the growth of a $LaAlO_3$ film on a $SrTiO_3$ substrate at an oxygen pressure of 37 mTorr. (**B**) RHEED pattern after the growth of a 10 unit-cell stoichiometric $LaAlO_3$ film. (**C**) AFM topographic images of the 10 unit-cell $LaAlO_3$ film on $SrTiO_3$. (**D**) Ti XAS spectra for a 10 unit-cell stoichiometric $LaAlO_3$ film. (**E**) Ti $L_{2,3}$-edges XLD spectra for 3 $LaAl_{1+y}O_{3(1+0.5y)}/SrTiO_3$ samples with y = -0.02, 0.00, and 0.08. (**F**) XMCD for 4 $LaAl_{1+y}O_{3(1+0.5y)}$ films with y = -0.02, 0.00, 0.06, and 0.08.

The high oxygen pressure helps to prevent the possible oxygen reduction in $SrTiO_3$, ensure that the $LaAlO_3$ films are sufficiently oxygenated. Figure 2D shows x-ray absorption spectroscopy (XAS) spectra with different linear polarizations and the Ti $L_{2,3}$ x-ray linear dichroism (XLD) signals are shown in Fig. 2E for different $LaAl_{1+y}O_{3(1+0.5y)}$ stoichiometry. No Ti^{3+} related features around 462 eV, which have been linked to oxygen deficiency,[6] are observed. Rather, the spectra are similar to the fully oxygenated samples.[6] Figure 2F shows the Ti $L_{2,3}$ x-ray magnetic

circular dichroism (XMCD) signals obtained from opposite circularly polarized XAS spectra. Very small XMCD signals were observed, consistent with the fully oxygen annealed samples and very weak ferromagnetism.[6]

In $LaAl_{1+y}O_{3(1+0.5y)}$, either Al vacancies or La vacancies in the off-stoichiometric films lead to oxygen vacancies in order to keep the charge neutrality.[5] As a result, the charge on the $[LaO_{1+y}]$ layer is $+(1-2y)$ and on the $[Al_{1+y}O_{2+0.5y}]$ layer is $-(1-2y)$. In the electronic reconstruction picture, instead of the charge transfer of half of an electron in the case of stoichiometric $LaAlO_3$, $(0.5-y)$ electrons will be transferred to resolve the polar discontinuity at the interface. The sheet carrier density depends linearly on y, *i.e.* $n_s = (1-2y)\times 3.3\times 10^{14}/cm^2$ for sufficiently thick $LaAlO_3$.[5] For the 10 unit-cell $LaAlO_3$ films used in this work, the dependence becomes $n_s = (1-2y)\times 3.3\times 10^{14}/cm^2 - 1.6\times 10^{14}/cm^2 = (1.7-2y\times 3.3)\times 10^{14}/cm^2$.[2]

The temperature and stoichiometry dependences of the sheet resistance, sheet carrier density, and mobility are shown in Fig. 3A-F, respectively, for the 10 unit-cell $LaAl_{1+y}O_{3(1+0.5y)}$ films. All of the films are conducting with sheet resistance around 10^4 Ω/□ at 300 K. The low temperature upturn has $-\ln T$ dependence characteristic of the Kondo effect. This may be attributed to the inevitable defects at the $LaAlO_3/SrTiO_3$ interface, consistent with the weak magnetism shown by Fig. 2F. The sheet carrier density is around $10^{14}/cm^2$ for all the samples, close to the expected value of $1.7\times 10^{14}/cm^2$.

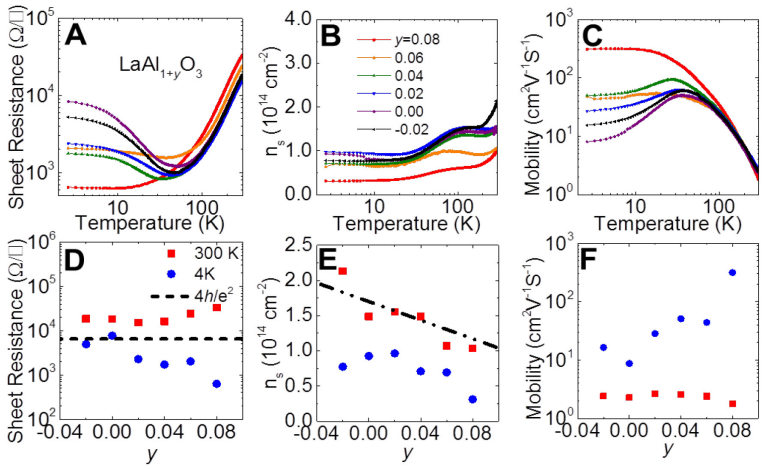

Figure 3 (**A**) Sheet resistance, (**B**) carrier density, and (**C**) Hall mobility as functions of temperature for a series of 10 unit-cell $LaAl_{1+y}O_{3(1+0.5y)}$ films. (**D**) Sheet resistance, (**E**) sheet carrier density, and (**F**) Hall mobility as functions of film stoichiometry at 300 K (red squares) and 4 K (blue dots). The dashed line in (**D**) is the quantum resistance limit $h/4e^2$. The dashed line in (**E**) indicates the theoretical value of sheet carrier density for 10 unit-cell films with different stoichiometry under the assumption of pure electronic reconstruction.[2]

The central result of our work is the dependence of sheet carrier density on the stoichiometry of $LaAl_{1+y}O_{3(1+0.5y)}$ shown in Fig. 3E. The black dashed line represents $n_s = (1.7-2y\times 3.3)\times 10^{14}/cm^2$, which is expected by the electronic reconstruction hypothesis for the 10 unit-cell films.[2] The red squares, which denote 300 K sheet carrier density, overlap with the dashed line. No additional mechanism is employed to explain our data. The quantitative agreement between our experimental result and the theoretical prediction provides a strong support to the electronic reconstruction mechanism. The key differences between our result and the previous reports are the high oxygen pressure during the film growth and the high film crystallinity. The high oxygen pressure suppresses the likelihood of oxygen vacancies in $SrTiO_3$. Well oxygenated samples produced during film growth can avoid possible defects when sufficient oxygen is provided only after the growth by annealing.

3. Strain-Engineered Oxygen Vacancies in $CaMnO_3$ Thin Films

Using ALL-Laser MBE, we synthesized high-quality singlec-rystalline $CaMnO_3$ films with systematically varying oxygen vacancy defect formation energies as controlled by coherent tensile strain. The systematic increase of the oxygen vacancy content in $CaMnO_3$ as a function of applied in-plane strain is observed and confirmed experimentally using high-resolution soft x-ray XAS in conjunction with bulk-sensitive hard x-ray photoemission spectroscopy (HAXPES). The relevant defect states in the densities of states are identified and the vacancy content in the films quantified using the combination of first-principles theory and core−hole multiplet calculations with holistic fitting. The strain-induced oxygen-vacancy formation and ordering are a promising avenue for designing and controlling new functionalities in complex transition-metal oxides.

Future Plans

The project has ended. Future funding will be sought to continue the research in oxide heterostructures using ALL-Laser MBE.

References

1. Hwang, H. Y. *et al*. Emergent phenomena at oxide interfaces. *Nature Mater.* 11, 103-113 (2012).
2. Cancellieri, C. *et al*. Electrostriction at the $LaAlO_3/SrTiO_3$ interface. *Phys. Rev. Lett.* **107**, 056102 (2011).
3. Siemons, W. *et al*. Origin of charge density at $LaAlO_3$ on $SrTiO_3$ heterointerfaces: possibility of intrinsic doping. *Phys. Rev. Lett.* **98**, 196802 (2007).
4. Ariando *et al*. Electronic phase separation at the $LaAlO_3/SrTiO_3$ interface. *Nat. Commun.* **2**,188 (2011).
5. Sato, H. K., Bell, C., Hikita, Y. & Hwang, H. Y. Stoichiometry control of the electronic properties of the $LaAlO_3/SrTiO_3$ heterointerface. *Appl. Phys. Lett.* 102, 251602 (2013).
6. Salluzzo, M. *et al*. Origin of interface magnetism in $BiMnO_3/SrTiO_3$ and $LaAlO_3/SrTiO_3$ heterostructures. *Phys. Rev. Lett.* **111**, 087204 (2013).

Publications

1. Guozhen Liu, Qingyu Lei, Matthäus A. Wolak, Qun Li, Long-Qing Chen, Christopher Winkler, Jennifer Sloppy, Mitra L. Taheri, and Xiaoxing Xi, Epitaxial strain and its relaxation at the $LaAlO_3/SrTiO_3$ interface, J. Appl. Phys. 120, 085302 (2016).
2. Ravini U. Chandrasena, Weibing Yang, Qingyu Lei, Mario U. Delgado-Jaime, Kanishka D. Wijesekara, Maryam Golalikhani, Bruce A. Davidson, Elke Arenholz, Keisuke Kobayashi, Masaaki Kobata, Frank M. F. de Groot, Ulrich Aschauer, Nicola A. Spaldin, Xiaoxing Xi,and Alexander X. Gray, Strain-Engineered Oxygen Vacancies in $CaMnO_3$ Thin Films, Nano Lett. 17, 794 (2017).
3. Qingyu Lei, Maryam Golalikhani, Bruce A. Davidson, Guozhen Liu, Darrell G. Schlom, Qiao Qiao, Yimei Zhu, Ravini U. Chandrasena, Weibing Yang, Alexander X. Gray, Elke Arenholz, Andrew K. Farrar, Dmitri A. Tenne, Minhui Hu, Jiandong Guo, Rakesh K Singh, X. X. Xi, Constructing oxide interfaces and heterostructures by atomic layer-by-layer laser molecular beam epitaxy, npj Quant. Mater. 2, 10 (2017).